A STUDY OF THE POTENTIAL ATTAINABLE GEOMETRIC ACCURACY OF IKONOS SATELLITE IMAGERY

Rongxing LI[1], Guoqing ZHOU[1], Songlin YANG[2], Grady TUELL[3], Nicholas J. SCHMIDT[4], Cindy FOWLER[4]
Department of Civil and Environmental Engineering and Geodetic Science.
[1]The Ohio State University, 470 Hitchcock Hall, 2070 Neil Avenue, Columbus, OH 43210-1275
Tel (614) 292-6946, Fax (614) 292-2957, Email: li.282@osu.edu
[2]North Jiaotong University, Beijing, China
[3]National Geodetic Survey, NOAA, [4]Coastal Service Center, NOAA

Working Group IV/6
HYPERLINK

ABSTRACT

This paper presents a study of the potential of the attainable accuracy of ground points from simulated IKONOS imagery. The details of the satellite image simulation are described, which include the satellite orbit, ground track, navigation data, the linear array imaging system, and the brightness of the satellite images at nadir- fore- and aft- views. A test field for evaluating the accuracy of the new generation high-resolution satellite was established in Madison County, in Central Ohio. This study assessed the accuracy of ground points versus the number and distribution of GCP, and versus the image measurement error of the GCP and checkpoints. From the experimental results obtained from the simulated satellite images and the established test fields, we conclude that the potential of this high-resolution (up to 0.82m) satellite imaging system will be able to meet the accuracy requirement for medium-scale topographic mapping, at least 1:24,000. The accuracy of ground points can reach 3m and 2m in planimetric and height dimensions. Also, some of suggestions for improving the accuracy of the ground points are made.

1. INTRODUCTION

Several commercial companies scheduled launches of high-resolution imaging satellites in the late 90' s. For example, EarlyBird (3m resolution, launched in early 1998 but failed two-way communication) and QuickBird (1m/4m resolution) from EarthWatch Inc. and OrbView-1 (1m/2m resolution) from Orbital Science Corporation, and IKONOS (0.82m resolution) from SpaceImaging/EOSAT. The new generation of commercial high-resolution satellites will revolutionize the work of photogrammetric and remote sensing communities (Fritz 1996), as these systems have the following obvious advantages over the current satellites: (1) high-resolution (up to 1m) imagery with long focal length, such as 10m in IKONOS; (2) enormous potential of their flexible pointing ability, such as, along-track stereo and cross-track stereo capabilities; (3) high geometric fidelity for linear array sensors with stereo imaging mode; (4) rapid conversion of image data into deliverable spatial information products; and (5) greater base-height ratio comparable to aerial photographs.

Elevation accuracy is crucial if satellite data are to be used to produce topographic mapping for national map products. SPOT satellite imagery products can only meet the requirements of small scale mapping at 1:50,000 and 1:100,000. Airborne photography is currently the primary technique employed in producing national map products. But, in spite of its advantages, such as high accuracy and flexible schedule (Li, 1998), it can not map areas where airplanes can not reach and its mapping frequency is constrained by the limits of flight planning. It is expected that the high-resolution satellite imagery such as that from IKONOS, have the potential for automatically extracting geographic information with the level of accuracy required by medium- and large-scale national digital mapping products (1:24 000 to 1:10 000). Moreover, this approach makes it possible to map an area frequently without the special flight planning and scheduling required by aerial photogrammetric data acquisition. This paper evaluates the potential attainable geometric accuracy of ground points derived from integrated GPS, INS and high-resolution satellite linear stereo image data (IKONOS). Various evaluation schemes are tried, such as geometric accuracy versus the number and distribution of GCPs, accuracy versus image measurement errors of GCPs and checkpoints. We used a test field for determining the 3D accuracy attainable from the new high-resolution satellite IKONOS-I. Prior to the accuracy assessment, we generated several simulated satellite images based on the IKONOS technical specification, DEMs and aerial photography of the test field .

Several researchers have done similar studies on three-line sensors in the MOMS series and HRSC nine-line sensors . Ebner et al. (1991) simulated the geometry and estimated the accuracy of MOMS-02/D2. Ebner and Strunz (1988) investigated the accuracy of ground points obtained using a DTM as control information. Ebner et al. (1992) performed a simulation study of the influences on the theoretical accuracy of the point determination from various factors, which included the precision of

observed exterior orientation parameters, the type and density of GCPs, the camera inclination across flight direction, and the simultaneous adjustment of two crossing strips with different intersection angles. The desired height accuracy of about 5m can be achieved by the simultaneous adjustment of two (or more) crossing strips within the overlapping area. Fraser and Shao (1996) did similar work evaluating the accuracy of ground points using MOMS data with different sets of control point configurations, numbers of orientation images and orders of interpolation functions using a control field in Australia. Habib and Beshah (1997) did their simulation study of an airborne Panoramic Linear Array Scanner. They concentrated on evaluating the effects of different numbers of GCP' s and different combinations of images. Fritsch et al. (1998) reported their recent result of processing MOMS-2P data so as to supply similar accuracies similar to MOMS-02/D2.

2. IMAGE SIMULATION OF IKONOS IMAGERY

The IKONOS Satellite is a typical representative of the linear stereo imaging systems. The satellite images the ground with nadir-, aft- and fore-looking angles. The generation of synthetic satellite images is based on the principle of projection and back-projection (see Figure 1)*Projection* is the processing the data from aerial images to the surface of a DEM, and *back-projection* is the same processing from the surface of a DEM to a satellite image at a fore-, nadir-, or aft- look. The brightness in the simulated satellite images is derived from the aerial images. Both of them share the identical DEM. To perform this simulation, the DEM data, aerial photographs, the technical specifications of IKONOS, and scene design are required.

2.1 Experimental Data

A DEM dataset in Madison County was derived from contour lines in DLG files from 7.5' USGS quad sheets, which were downloaded from the USGS website. The DEM was interpolated to a 1m by 1m spacing using ARC/INFO.

The Center for Mapping of the Ohio State University provided us with the aerial images. They were acquired in 1997 by the AIMS (Airborne Integrated Mapping System) using a digital camera with a focal length of 50 mm and an image size of 4,096 by 4,096 pixels (60 by 60 mm imaging area resulting in a 15 micron pixel size). The flying height is about 1366m and the ground sample distance (GSD) is around 0.409 m (Figure 4).

The details of the system characteristics and imaging geometry of IKONOS have been described in Li et al. (1999). Table 1 lists the specifications of IKONOS used for this simulation.

Parameter	Values	Parameter	Values	Parameter	Values
Altitude (km)	680	Convergence angle (deg)	45	Ground resolution (m)	0.82
Inclination (deg)	98.1	Pixel size (μm)	12	Swath width (km)	11

Table 1. Technical specifications of IKONOS used for the experiment

It is necessary to select an area within the established test field in which the aerial photography and corresponding DEM are available. Also, a reference point is selected as the start position of the satellite trajectory. From the reported specification of IKONOS, the orbit inclination is 98.1 degrees, so the angle κ = 98.1 degrees was set for the azimuth and used during the image generation. The satellite will be traveling from north to south at a speed of 7000m per second. The velocity vector has to be decomposed into the components along the x-axis and y-axis, neglecting any component in z direction. Table 2 shows the simulated exterior parameters at an initial time and after 5 seconds for the fore-, nadir- and aft- looks. With an altitude of 680 km and focal length of 10m, the GSD is around 0.816m.The coverage of an aerial photography is 1676.6 by 1676.6m, and the size of a satellite image is designed to be 2000 by 2000 pixels. Figure 2 shows the geometric relationships between the orientation of the satellite orbit, ground coordinate system and the image coordinate system.

Parameter	Sigma	Fore-look		Nadir-look		Aft-look	
		Initial	At 5″	Initial	At 5″	Initial	At 5″
Xs (m)	3.0	330459.9	365125.3	284315.7	318981.1	238171.5	272830.6
Ys (m)	3.0	4096476.8	4091613.1	4424815.0	4419951.1	4753153.2	4748289.4
Zs (m)	3.0	679996.87	679996.6	679996.87	679999.6	679996.8	679998.9
Omega (arc sec)	2.0	0.000020	-0.000157	0.000020	-0.006215	0.000010	-0.000633
Phi (arc sec)	2.0	0.000020	0.000022	0.000020	-0.000931	0.000010	0.00001
Kappa (arc sec)	2.0	0.139636	0.139560	0.139647	0.139749	0.139647	0.144059

Table 2. Exterior orientation parameters of a segment of a simplified orbit

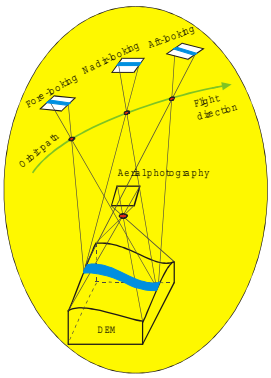

Figure 1. Generation of synthetic satellite images based on the aerial images, DEM and technical parameters of IKONOS

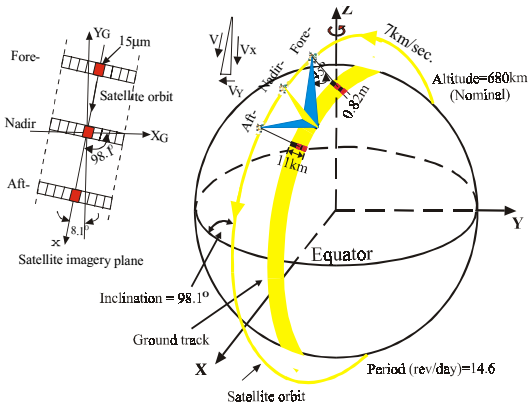

Figure 2. Geometric configuration of the satellite image simulation

2.2 The Brightness on the Satellite Imagery

Assuming that the coordinates of any point in the image plane at the nadir look is (x_1, y_1), its corresponding ground coordinates are determined by

$$v_{Z_k} = Z_k - Z_k(X_k, Y_k) \tag{1}$$

where v_{Z_k} is the residual of Z_k, $Z_k(X_k, Y_k)$ denotes the elevation from the DEM, and X_k, Y_k, Z_k are unknown coordinates of the ground point P_k. In the case of a grid DEM, the elevation of an arbitary point is interpolated from its neighbor grid points. A bilinear interpolation can be used to calculate this elevation from the surrounding 4 grid points (see Figure 3):

$$Z_k(X_k, Y_k) = (1-C_1)(1-C_2)Z_{i,j} + C_1(1-C_2)Z_{i+1,j} + (1-C_1)C_2Z_{i,j+1} + C_1C_2Z_{i+1,j+1} \tag{2}$$

where $C_1 = (X_k - X_i / L)$, $C_2 = (Y_k - Y_i / L)$, $L = (X_{i+1} - X_i) = (Y_{j+1} - Y_j)$ is a constant of grid width. The linearization of equation (1) using the initial values, X_k^o and Y_k^o, yields

$$v_{Z_k} = a_1\Delta X_k + a_2\Delta Y_k + a_3\Delta Z_k - l_k, \tag{3}$$

where:

$$a_1 = -\frac{(1-C_2^o)}{L}Z_{i,j} + \frac{(1-C_2^o)}{L}Z_{i+1,j} - \frac{C_2^o}{L}Z_{i,j+1} + \frac{C_2^o}{L}Z_{i+1,j+1}$$

$$a_2 = -\frac{(1-C_1^o)}{L}Z_{i,j} - \frac{C_1^o}{L}Z_{i+1,j} + \frac{(1-C_1^o)}{L}Z_{i,j+1} + \frac{C_1^o}{L}Z_{i+1,j+1}$$

$$a_3 = 1.0,\ l_k = Z_k^o - Z_k(X_k^o, Y_k^o),\ C_1^o = -\frac{(X_k^o - X_i)}{L},\ C_2^o = -\frac{(Y_k^o - Y_i)}{L}$$

The value $Z_k(X_k^o, Y_k^o)$ is dervived from approximate values X_k^o and Y_k^o, which change in each iteration. Therefore, the observation also varies from iteration to iteration.

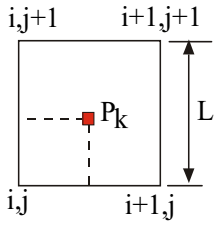

Figure 3. Bilinear interpolation using 4 surrounding grid points

When the ground coordinates X_k, Y_k, Z_k are known, the corresponding image coordinates (x'_1, y'_1) in the aerial image can be determined by back-projection (from DEM to the aerial image), when the image' s interior and exterior orientation parameters and calibration parameters are available. The brightness $G(x'_1, y'_1)$ at (x'_1, y'_1) in the aerial image is assigned the value at (x_1, y_1) of the satellite image. In this way, the brightness of each point in the one-dimensional linear array can be obtained by repeating this process.

Using the pushbroom imaging principle for a satellite traveling at speed of 7000m per second at a 680km flying height, a successive one-dimensional linear array image was simulated along the direction of flight. In this way, we produced a simulated scene at the nadir look (see Figures 5). Similarly we can obtain the simulated images at fore-, and aft-looks (see Figures 6 and 7).

Figure 4. Original aerial image (GSD: 0.4m)

Figure 5. Simulated nadir-look image (GSD: 0.82m)

Figure 6. Simulated fore-look image (GSD: 0.82m)

Figure 7. Simulated aft-look image (GSD: 0.82m)

EMBED

2.3 Errors in the simulated images

The simulation of satellite imagery done here is only for the purpose of photogrammetric positioning, while the real satellite imaging system is much more complex than we have assumed above. For example, a nonlinear mathematical model of orbital dynamics would be needed to calculate how the earth rotation, moon and planet perturbation, and atmospheric refraction, truly impact the positional accuracy of each pixel in the image plane. Besides, the accuracy of the grid DEM derived from the DLG data also influences the positional accuracy of each pixel. This type of errors results in the rough edges (see Figure 8). Moreover, the downloaded DLG data from USGS 1:24,000 scale topographic quadrangle maps were produced in 1979, while the aerial photography was taken in 1997. The 18-year interval between DEM and aerial photography will probably result in some positional errors.

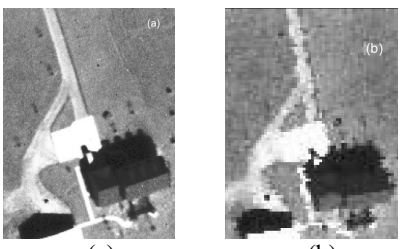

(a) (b)

Figure 8. (a) Original aerial photography with GSD of 0.41m; (b) simulated satellite image with a GSD of 0.82m at a nadir look

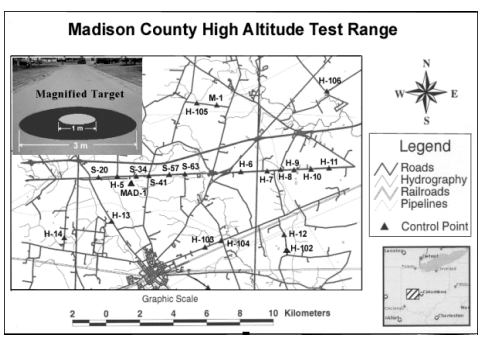

Figure 9. The distribution of GCP and the target point pattern at The High Altitude Test Range in Madison, OH

3. TEST FIELD ESTABLISHMENT

3.1 The High Altitude Test Range

The High Altitude Test Range for evaluating the potential accuracy of the new generation satellite imagery was established in Madison County, Central Ohio by the cooperation of the Ohio Department of Transportation (ODOT) and OSU. The control network, which consists of 21 ground target points plus the 3 higher-order control points, was specifically distributed in a flat area approximately 16x11 km, centered at latitude 39°56' 24 North, and longitude 83°24' 42 West along in an east-west direction. The target points are spaced at least 1 km apart. All target points are painted with concentric circles, a one-meter flat white circle and a three-meter flat black circle as background, centered on a monument (see Figure 9). Additionally, 24 checkpoints were also surveyed for the purpose of testing the attainable accuracy of the linear array satellite data.

In static mode, each station of 24 control points was observed by a Trimble GPS receiver for least 2 hours in order to insure that at least 4 GPS range observations were locked. In fast static mode, the observations of each station of 23 checkpoints were made. In this case, MAD-1 is used as the reference. Feature points are mainly selected at intersections of roads, bridges, and distinct permanent marks.

Finally, geographic coordinates in the WGS-84 and UTM systems were obtained. The standard errors of these control points reached 0.02, 0.02 and 0.10 meter in latitude, longitude and elevation respectively.

3.2 The second test field

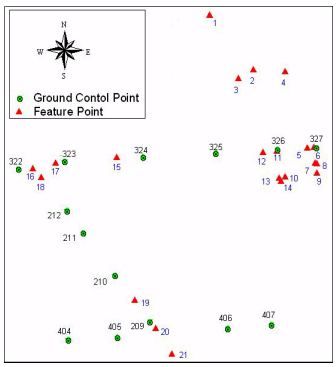

Figure 10. The distribution of GCPs and feature points at the Second Test Field

The second test field is also locate in Madison county, but covers only 2km by 2km and lies within an area covered by AIMS images(Figure 10). In this test field, 14 target control points were measured by ODOT. In fast static mode, we used 2 Trimble 4000SSI receivers to measure 21 feature points, which specifically appear at the intersection of roads, or permanent marks. These feature points could be recognized easily in aerial images. The higher order control point, MAD-1, (PID: AB6042 from the National Geodetic Survey) was used as a reference station. The observation time of each station depends on the number of satellites locked. If 4 satellites are locked, at least 20 minutes are required; if the 6 satellites are locked, at least 8 minutes. Finally, the coordinates of 21 feature points in various coordinate systems, UTM, SPC and WGS84, can be obtained by computation with the software GPSurvey. The accuracy of all baselines achieved millimeter level. This level of accuracy is enough to meet our accuracy requirement for testing (Gonzalez 1998).

4. POTENTIAL ATTAINABLE ACCURACY OF GROUND POINTS FROM IKONOS

4.1 Accuracy Assessment based on the High Altitude Test Range

We used 24 GCPs (21 *high altitude* ground target points plus three higher-order control points) and 14 checkpoints. Their 2D image coordinates in the satellite image planes at nadir- aft- and fore- looks are computed by the rigorous mathematical model of bundle adjustment, and then random errors (1 sigma) are added to the following simulated parameters

- Position of OLs (Orientation Lines): 3m
- Attitude of OLs: 2 arc second
- Measured image coordinates of GCPs: 0.5 pixel

The following accuracy assessment is conducted based on the above conditions.

Accuracy versus various number of GCPs: The ground coordinates of 14 checkpoints were computed by the bundle adjustment program. Differences between the computed and known ground coordinates of the 14 checkpoints are depicted in Figure 11 with a variation in the number of GCPs used. The average planimetric and vertical absolute error can reach 11

to 12 m without any GCPs, and around 2.8 m with 24 GCPs. When 4 GCPs are used, the accuracy is greatly improved. However, using more than 4 GCPs does not contribute significantly to the accuracy. Thus it is not encouraged that one try to improve the geometric accuracy by significantly increasing the number of GCPs.

Accuracy versus distributions of GCPs: Figure 13 shows the GPS network. We chose 6 groups of GCPs to form 6 distributions in order to examine the impact of GCP distribution on accuracy. The 6 distributions are:

Distribution 1: a triangle consisting of points MAD-1, BLT-0 and H-34;
Distribution 2: a trapezoid formed by points H-34, BLT-0, H-105 and H-106;
Distribution 3: approximately a straight line (cross track) formed by points H-105, M-1 and H-106;
Distribution 4: Points S-20, H-5, S-34, MAD-1, S-41, S-57, S-63, H-6, H-7 and H-11 spread out over the area;
Distribution 5: Points H-34, H-14, H-13, H-12 and BLT-0 approximately on a straight line (cross track);
Distribution 6: Points S-20, S-34, S41 and S-57 approximately on a straight line (cross track).

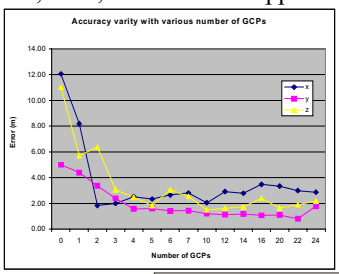

Fig. 11. Accuracy vs. number of GCPs

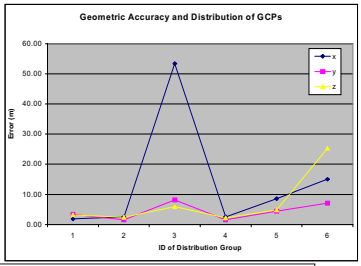

Fig. 12. Accuracy vs. GCP distribution

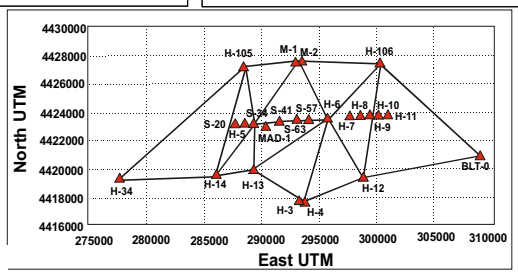

Fig. 13. The distribution of GCPs at the Test Range

The accuracy of the ground coordinates of the 14 checkpoints versus the 6 distributions of GCPs is depicted in Figure 12. We find that the strength of the GCP distributions affects the planimetric and vertical accuracy significantly. For example, Distribution 1 and 3 has the same number of GCPs, but different distributions. The geometric accuracy for Distribution 1 achieves 1.84m and 3.43m in X and Y, and 3.21m in Z, while Distribution 3 has 53.4m and 8.11m in X and Y, and 5.88m in Z. Distribution 2 and 6 present a similar situation. We note that GCPs distributed on a straight line across the track constitutes a weak geometric configuration (Distributions 3, 5 and 6). Thus GCP distribution is a critical factor for achieving high accuracy.

EMBED

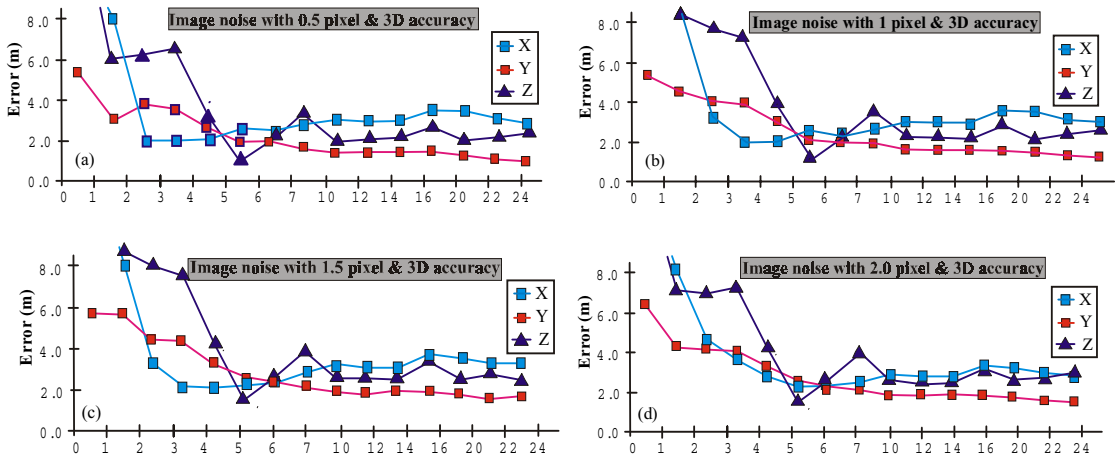

Figure 14. Accuracy versus errors in image coordinates

Accuracy versus image measuring errors of checkpoints: When measuring image coordinates in a stereo pair, errors are unavoidable. The impact of these errors on ground coordinates should be assessed. Suppose that image coordinate measurement errors range from 6μm (0.5 pixel) to 24μm (2 pixel), and all other parameters are noise-free. The ground coordinate accuracy of 14 checkpoints versus errors in image coordinates is depicted in Figure 14. The result demonstrates that large measurement errors in image coordinates affect accuracy of ground coordinates. Indeed, the planimetric coordinate errors increase 0.5m for each error of 0.5 pixels in image coordinates.

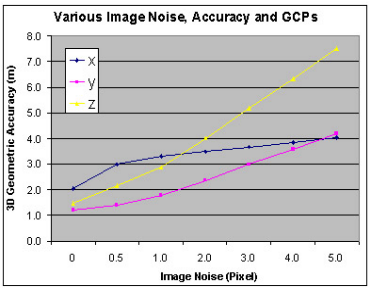

Figure 15. Accuracy versus errors of image coordinates

Accuracy versus errors of image coordinates of GCPs: Under the same condition as above, we examine the impact of image coordinate errors of GCPs on ground coordinate accuracy. The errors of ground coordinates for 14 checkpoints are shown in Figure 15. When image coordinate errors are 5 pixels, Z coordinate error reaches 7.7 m and X and Y errors are around 4 m even though all of 24 GCPs are taken as control information. Obviously precisely locating and measuring of GCPs in images is helpful to improve accuracy.

4.2 Accuracy Assessment based on the Second Test Field

In the second test field, all target points and feature points on aerial image AIMS 1185, can clearly be recognized. In order to perform further processing, each target point and feature point on the aerial image is marked by a cross of 5 by 5 pixels (see Figure 16) in order that all target points and feature points can still be recognized in simulated satellite images. Unfortunately, The target point 212 and feature points 3, 7 and 20 can not be located correctly because the out-of-date DEM (created in 1979), which would not correspond to the aerial image taken in 1997. The following experiments conducted are based on the above condition. No random noise is added to any parameters.

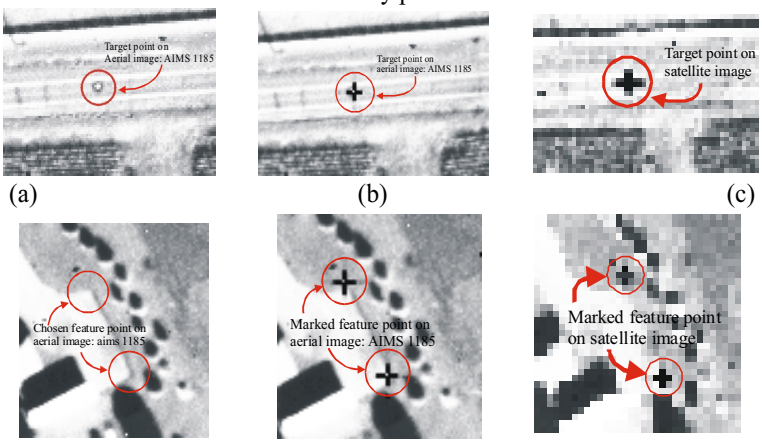

Figure 16. Target points and feature points as well as their marks on aerial image AIMS 1185 and simulated satellite image

Accuracy versus various numbers of GCPs: The ground coordinates of 18 feature points were computed by the bundle adjustment program. Differences between the computed coordinates and the ground coordinates measured by GPS are listed in Table 3. The average RMS can reach 11 m in x and 38m in y and 13 m in z without GCPs, and around 2.7 m in x and 1.6 m in y and 1.99 m in z with 13 GCPs. When 3 spare GCPs, which cover the whole image 1185, are used, the accuracy is largely improved. However, more than 7 GCPs do not contribute the accuracy significantly. This result is similar to the one above for the first test field.

Number	Point ID (see Figure 8)	RMSx	RMSy	RMSz
0		10.67	38.55	13.41
1	(324)	4.97	30.63	2.35
2	(324, 209)	5.07	30.63	2.11
3	(324, 209, 327)	4.89	1.85	3.98
7	(322, 209, 327, 1, 323, 407, 404)	3.18	1.58	2.06
13	(above 7 points + 405, 406, 210, 212, 2, 325)	2.74	1.57	1.99

Table 3. Experimental result of accuracy versus number of GCPs in the second test field

Accuracy versus distributions of GCPs: 6 distributions are constructed in order to examine the impact of GCP distribution on accuracy. The accuracy of 18 feature points with respect to various distributions is listed in Table 4. We find that the strength of the GCP distributions affects the planimetric and vertical accuracy significantly. For example, Distributions 2 and 3 have the same number of GCPs, but different distributions. The accuracy of Distribution 2 achieves 3.82 m and 1.79 m in X and Y, 2.19 in Z, while Distribution 3 has 25.46 m and 15.96 m in X and Y, and 34.47 m in Z. It should be noted that GCPs distributed on a straight line across the track, such as Distributions 3, and 6, constitutes a weak geometric configuration. Thus, an appropriate GCP distribution is critical to achieve high accuracy.

Distribution number	Point ID for Distribution of GCP (see Fig. 8)	RMSx	RMSy	RMSz
1	327,404	6.77	39.06	4.58
2	209,327,322	3.82	1.79	2.19
3	407,209,404	25.46	15.96	34.47
4	407, 326, 1	5.74	1.74	4.44
5	327, 322, 407, 404	3.42	1.59	2.07
6	322, 323, 324, 325, 326, 327	75.92	1.91	36.07

Table 4. Experimental result of accuracy versus distribution of GCPs in the second test field

5. CONCLUSIONS

From the results obtained with the simulated satellite images covering the established test field, some encouraging conclusions can be drawn about the mapping potential of this high resolution satellite image system. The accuracy of ground points can reach 3m in planimetry and 2m in height with over 4 GCPs in spite of fact that the experimental conditions were based on a simulated study. Therefore, significantly more than four GCPs are not recommended in order to maintain high accuracy and minimize costs. A distribution of GCPs along a straight line, especially across the track, is not useful for increasing the accuracy of ground points. A well spread distribution of even a few GCPs is more beneficial to accuracy improvement than a dense but poorly spread distribution. The one-meter resolution imagery will meet accuracy requirement for medium-scale topographic mapping at scales from 1:24,000 to 1:10,000.

ACKNOWLEDGMENTS

We appreciate the funding from the Sea Grant NOAA National Partnership Program. Funding and assistance from CSC, OCS, and NGS of NOAA are appreciated. We would like to acknowledge the assistance in the GPS survey from Mr. David Albrecht of the Ohio Department of Transportation (ODOT) and Dr. Dorota Grejner-Brezezinska of the Center for Mapping. Discussions with Mr. David Conner, NOAA geodetic advisor to Ohio, on geodetic datum issues were very helpful.

REFERENCES

Ebner, H. and Strunz, G., 1988. Combined Point Determination Using Digital Terrain Models as Control Information. In: Int. Archives of Photogrammetry and Remote Sensing, Vol. 27, Part B11, pp. III/578-587.

Ebner, H., Kornus, W., Strunz, G., 1991. A Simulation Study on Point Determination Using MOMS-02/D2 imagery. Int. Journal of PE & RS, 57 (10), pp.1315-1320.

Ebner, H., Kornus, W., Ohlhof, T., 1992. A Simulation Study on Point Determination For The MOMS-02/D2 Space Project Using An Extended Functional Model. In: Int. Archives of Photogrammetry and Remote Sensing, Vol.29, Part B4, pp.458-464.

Ebner, H., Ohlhof, T., Putz, E., 1996. Orientation of MOMS-02/D2 and MOMS-2P Imagery. In: Int. Archives of Photogrammetry and Remote Sensing, Vol. XXXI, Part B2, pp. 158- 164.

Folchi, W., 1996. Satellite Orthoimagery: Mapping the Future Today, The Space Imaging Approach. In: Proceedings of ACSM/ASPRS Annual Conf. & Exposition, Baltimore, MD, Vol.2, pp.74-81.

Fraser, C. and Shao, J., 1996. Exterior Orientation Determination of MOMS-02 Three-Line Imagery: Experiences with the Australian Testified Area. In: Int. Archives of P&RS, Vol. XXXI, Part B3, pp.207-214.

Fritsch, D., Kiefner, M., Stallman, D., Hahn, M., 1998. Improvement of the Automatic MOMS02-P DTM Reconstruction. Int. Archive of Photogrammetry and Remote Sensing, Vol. 32, Part 4, GIS-Between Visions and Applications, Stuttgart, Germany, pp.170-175.

Fritz, L.W., 1996. Commercial Earth Observation Satellite. In: Int. Archives of Photogrammetry and Remote Sensing, Vol. XXXI Part. B4, pp.273-282.

Gonzalez, R. A., 1998. Horizontal Accuracy Assessment of the New Generation of High Resolution Satellite Imagery for Mapping Purposes. M.S. Thesis, Graduate Program of Geodetic Science and Surveying, The Ohio State University.

Habib, A. and Beshah, B., 1997. Modeling Panoramic Linear Array Scanner. Report No. 443, Department of Civil and Environmental Engineering and Geodetic Science, The Ohio State University, Columbus, OH.

Kornus, W. and Lehner, M., 1998. Photogrammetric point determination and DEM Generation Using MOMS-2P/PRIRODA three-line Imagery. In: Int. Archives of Photogrammetry and Remote Sensing, Vol. 32, Part 4, Stuttgart, Germany, pp.321-328.

Li, R., Zhou, G., Gonzalez, A, Liu, J. K., Ma, F., Felus, Y., Lapine, L., Lockwood, M., Schmidt, N. J., Fowler, C., 1998. Coastline Mapping and Change Detection Using One-Meter Resolution Satellite Imagery. Project Annual Report, Department of Civil and Environmental Engineering and Geodetic Science, The Ohio State University, Columbus, OH.

Li, R. and Zhou, G., 1999. Experimental Study On Ground Point Determination From High Resolution Airborne And Satellite Imagery. ASPRS annual conference, Portland , pp.88-97.

Parker, J., 1997. The Advantages of In-Track Stereo Acquisition from High-Resolution Earth Resources Satellites. In: Proceedings of ACSM/ASPRS Annual convention & Exposition, Seattle, WA, Vol.3, pp.276-282.